Beneficial Role of a Bulky Donor Moiety in π-Extended Organic Dyes for Mesoscopic TiO2 Sensitized Solar Cells

RESEARCH · MAY 2015

DOI: 10.13140/RG.2.1.1562.5125

THE JOURNAL OF PHYSICAL CHEMISTRY C

Article

pubs.acs.org/JPCC

Beneficial Role of a Bulky Donor Moiety in π-Extended Organic Dyes for Mesoscopic TiO_2 Sensitized Solar Cells

Vittoria Roiati,[†,‡] Roberto Giannuzzi,[†] Giovanni Lerario,[†] Luisa De Marco,[†] Rita Agosta,[†] Rosabianca Iacobellis,[†,#] Roberto Grisorio,[§] Gian Paolo Suranna,[§] Andrea Listorti,*[,†,∥] and Giuseppe Gigli[†,▽,⊥]

[†]Center for Bio-Molecular Nanotechnology, Fondazione Istituto Italiano di Tecnologia, Via Barsanti, 73010 Arnesano (Lecce), Italy

[‡]Department of Physics, Politecnico di Milano, Piazza Leonardo da Vinci 32, Milano, Italy

[§]Dipartimento di Ingegneria Civile, Ambientale, del Territorio, Edile e di Chimica (DICATECh), Politecnico di Bari, Via Orabona, 4 I-70125 Bari, Italy

[∥]NNL—National Nanotechnology Laboratory, CNR Istituto Nanoscienze, Distretto Tecnologico, Via Arnesano 16, 73100 Lecce, Italy

[⊥]Dipartimento di Matematica e Fisica "E. De Giorgi", Universita' del Salento, Via per Arnesano, 73100 Lecce, Italy

[#]Dipartimento di Ingegneria dell'Innovazione, Universita' del Salento, Via per Monteroni, 73100 Lecce, Italy

[▽]CNR IMIP, Distretto Tecnologico, Via per Arnesano, 73100 Lecce, Italy

Supporting Information

ABSTRACT: This paper reports the spectroscopic and electrochemical characterization of two π-extended D−A−π−A organic dyes, G1 and G2, along with a comparison with their donor-free congeners, DTB-T and DTB-B. A collection of measurements has been carried out to provide insight into the different processes (injection, regeneration, and recombination) involved in the photovoltaic conversion. The study aims, in particular, at rationalizing how the presence of a bulky triarylamine donor group, along with the modification in the chemical structure of the π-bridge, influences the operative cycle of dye-sensitized solar cells. We demonstrated that the donor group contributes to the formation of a more robust organic layer uniformly covering the TiO_2 surface, thus decreasing unfavorable charge recombination processes. In addition, the presence of the thiophene sulfur atom in one of the dye π-extensions (G1), by favoring interactions with the triiodide in the electrolyte, triggers detrimental recombination pathways. We conclude from these observations that G2, the sensitizer with a non-thiophene π-extension, possesses the highest photovoltaic performances among the investigated sensitizers.

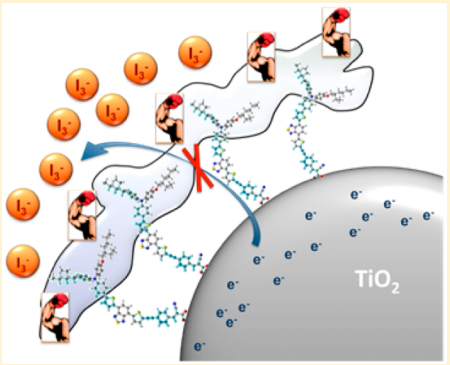

INTRODUCTION

Sunlight is arguably the most abundant clean energy source capable of enabling sustainable economic growth, with a minimum detrimental impact on the environment.[1] There are many innovative solar cell technologies that promise cheap solar power solutions and possess characteristics suitable for various technological applications. Among these alternatives to silicon technologies, dye-sensitized solar cells (DSSC)[2−4] are overwhelmingly coming of age, opening up potential penetration into high added value energy markets, such as the so-called BIPV (building-integrated photovoltaics) unattainable by classic inorganic semiconductor based photovoltaics.

At the core of a DSSC lays the dye (sensitizer), which governs light harvesting and the generation of free carriers after electron injection into the conduction band of the nanostructured semiconducting oxide. In addition, the sensitizer structure has been shown to control key electron transfer processes at the TiO_2/dye/electrolyte interface, such as the recombination of injected electrons with electrolyte constituents or with the dye cations themselves.[5] For this reason, huge efforts have focused on the development of new efficient sensitizers that could improve device performances, progressing in the roadmap toward the prospective widespread applications of this technology. While ruthenium dyes[6] have long been considered for high-performance applications, the low abundance of this metal and the modest molar extinction coefficients of ruthenium complexes limit their performances when employed for the sensitization of thin electrodes. This drawback is particularly critical in the case of DSSCs based on solid-state or ionic liquid electrolytes, as a thin electrode is the fundamental requirement of such approaches.[7,8] To overcome

Received: December 4, 2014
Revised: February 23, 2015
Published: March 4, 2015

DOI: 10.1021/jp5121004
J. Phys. Chem. C 2015, 119, 6956−6965

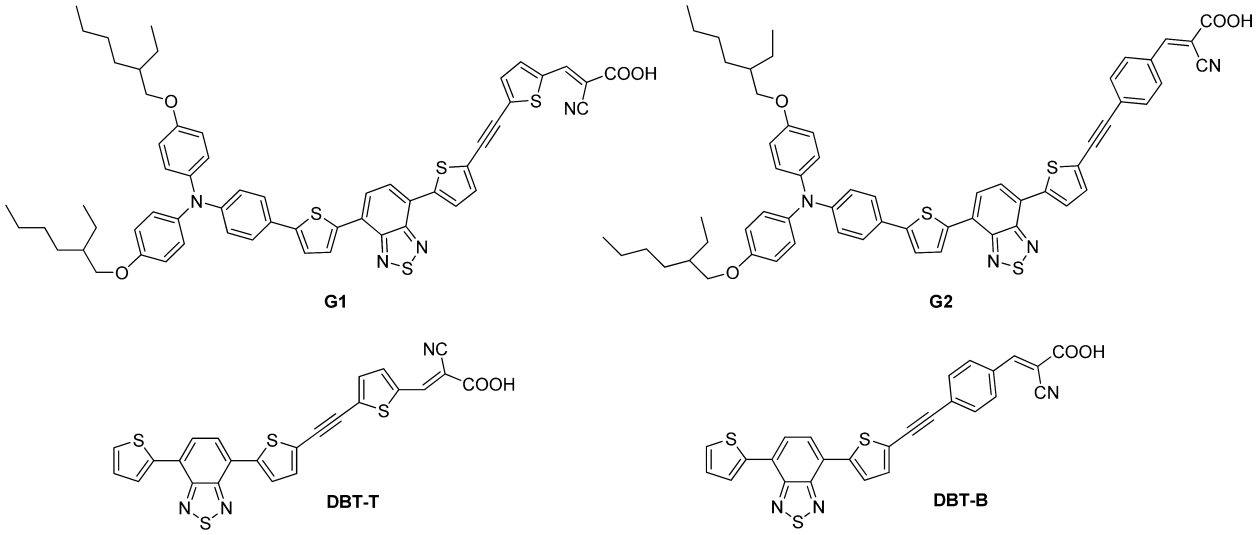

Figure 1. Structures of the two dyes (G1 and G2) and of their donor-free analogues (DTB-B and DTB-T).

this problem, the use of organic sensitizers is a useful strategy. These dyes have attracted great interest because of their large molar absorption coefficients and for the potentially low production costs associated with their easier synthesis.[9] Many different organic dyes with conversion efficiencies in the range of 6−9% have been reported in the last few years, but only a few examples have breached the 10% efficiency limit.[10] Concerning device stability, organic DSSC have recently reached the 2200 h limit, confirming their potential in terms of practical applications.[11]

The donor−π-bridge−acceptor (D−π−A) configuration is mainstream in the design of organic sensitizers due to its ability to promote modulation of the photoinduced charge separation. An evolution of this concept has led to the awareness that incorporating an electron-withdrawing unit within the π-bridge, as a further internal acceptor (leading to D−A−π−A organic sensitizers), displays several advantages, such as the tuning of the molecular energy levels, the red-shift of the charge-transfer absorption band, and a distinct improvement of the photovoltaic (PV) performance as well as photo- and thermostability of the sensitizers.[12] Benzothiadiazole has been recognized as one of the most versatile units for this purpose and has therefore been widely employed in the synthesis of high-efficiency D−A−π−A dyes.[13−15]

Notwithstanding the consistent progresses made, the necessary further development of organic sensitizers requires a better understanding of the relations between the structure of a dye and its PV performance. In this framework, starting from a parent structure,[15] two π-extended benzothiadiazole-based D−A−π−A dyes have been recently modeled, synthesized, and tested in devices. These sensitizers were characterized by an electron-donating triarylamine group, a dithienyl-benzothiadiazole chromophore, a suitable π-bridge extension constituted by an ethynylene−thienylene and an ethynylene−phenylene group (G1 and G2, respectively, Figure 1), and a cyanoacrylic anchoring moiety. This structural modification enabled, when employed in liquid electrolyte DSSC, reaching conversion efficiencies as high as 8.1%, in the case of G2. In parallel, the need to mitigate the typical "camelback" profile absorption effect of benzothiadiazole dyes, which limits the light harvesting in the UV−vis region between 400 and 500 nm, motivated us to investigate a molecular tailoring of G1 and G2. A viable strategy was identified in the suppression of the donor group. The donor-free congeners of G1 and G2 (Figure 1, DTB-T and DTB-B, respectively) have been synthesized for generating a highly efficient multisensitizer system. These donor-free cosensitizers show, in fact, a complementary UV−vis absorption with respect to G1 and G2. The G2/DTB-T 2:1 (mol/mol) multisensitizer system allowed efficiencies higher than the sum of those of the individual dyes to be reached, as well as superior electron lifetimes. Those results indicated an efficient coverage of the TiO_2 surface, an increased light harvesting of the photoelectrode, and a sensible suppression of the recombination phenomena.[16,17]

The reported outcomes deserved, in our opinion, a further in-depth investigation aimed at elucidating the obtained results from a photophysical point of view. Therefore, we scrutinized, through a complete spectroscopic and electrochemical investigation carried out on operative devices, the classic (G1 and G2) and donor-free (DTB-T and DTB-B) dyes. By isolating the different steps (injection, regeneration, and recombination) involved in the PV conversion, the aim of this study is to rationalize in particular how the presence of a bulky triarylamine donor group and the modification in the chemical structure of the π-bridge influence these basic steps of the DSSC operative cycle.

EXPERIMENTAL SECTION

Synthesis. The syntheses of G1, G2, DTB-T, and DTB-B have been carried out according to literature procedures.[16,17]

Fabrication of DSSC and Photovoltaic Measurement. Glass plates of fluorine-doped tin oxide (FTO, 15 Ω/sq, provided by Solaronix S.A.) were first cleaned for 15 min in a detergent solution under ultrasound stirring and then rinsed with water and ethanol. Double-layer photoanodes of ∼17 μm thickness were prepared by (i) depositing a layer of commercial colloidal paste (Dyesol 18NR-T) onto the FTO glass and then drying at 125 °C for 15 min, obtaining a transparent nanocrystalline film (∼12 μm); (ii) depositing a ∼5 μm scattering layer (Solaronix D/SP colloidal paste) on top of the transparent layer; and (iii) performing a sintering process at 450 °C for 30 min. The dye loading was performed by keeping the photoelectrodes in the dark for 14 h in 0.2 mM THF solutions of G1, G2, DTB-T, and DTB-B sensitizers containing

DOI: 10.1021/jp5121004
J. Phys. Chem. C 2015, 119, 6956−6965

80 mM of chenodeoxycholic acid (CDCA) as coadsorbent. The counter electrodes were prepared by sputtering a 50 nm Pt layer on a hole-drilled, cleaned FTO plate. In a typical device construction procedure, the photoanode and the counter electrode were faced and assembled using a suitably cut 50 μm thick Surlyn hot-melt gasket for sealing. The redox electrolyte (0.1 M LiI, 0.02 M I_2, 0.6 M 1-methyl-3-propylimidazolium iodide, and 0.5 M *tert*-butylpyridine in dry acetonitrile) was vacuum-injected into the space between the electrodes through holes suitably predrilled on the back of the counter electrode. The devices were completed by sealing holes with a Surlyn hot melt film and a cover glass.

Simplified working devices used in the photoinduced absorption (PIA), transient photovoltage (TPV), and electrochemical impedance spectroscopy (EIS) investigations were fabricated as follows: single-layer transparent photoelectrodes (overall thickness ~6 μm) were prepared by doctor-blading commercial titania paste onto the FTO glass, gradually heating the films under air in an oven up to 450 °C, and then performing a sintering process for 30 min; the counter electrodes were prepared by sputtering a 10 nm Pt layer on a hole-drilled, cleaned FTO plate. Dye loading and device assembly was carried out as previously described.

Samples for time-correlated single-photon counting (TCSPC) were prepared using transparent TiO_2 photoanodes (3 μm) or Al_2O_3 films (5 μm) sensitized with 0.02 mM THF solution of the dyes containing 8.0 mM CDCA and FTO as counter electrodes, assembled as a sandwich-type cell, and filled with redox electrolyte as previously described.

Photocurrent−voltage measurements were performed using a Keithley unit (model 2400 Source Meter). A Newport AM 1.5 solar simulator (model 91160A equipped with a 1000 W xenon arc lamp) served as a light source. The incident light intensity was calibrated to 100 mW cm^{-2} using a reference silicon solar cell. The incident photon-to-current conversion efficiency (IPCE) was measured by the dc method using a computer-controlled Xenon arc lamp (Newport, 140 W, 67005) coupled with a monochromator (Newport Cornerstore 260 Oriel 74125). The light intensity was measured by a calibrated silicon UV-photodetector (Oriel 71675), and the short circuit currents of the DSSCs were measured by using a dual-channel optical power/energy meter (Newport 2936-C).

Electrochemical impedance spectroscopy (EIS) was performed by an AUTOLAB PGSTAT 302N (Eco Chemie B.V.) in a frequency range between 100 kHz and 10 mHz. The impedance measurements were carried out at different voltage biases under 1.0 sun illumination. The resulting impedance spectra were fitted by using ZView (Scribner Associates) software.

Time-resolved photoluminescence measurements were carried out using a time-correlated single-photon counting (TCSPC) apparatus comprising a Edinburgh FLS980 spectrometer using a laser diode as excitation source (1 MHz, λ_{exc} = 405, 515, or 635 nm, 20−100 ps time resolution after deconvolution) and an MCP as detector. Photoinduced absorption (PIA) spectra were recorded using a white light probe generated by a 250 W tungsten−halogen lamp which was superimposed to a Spectra Physics square-wave modulated laser source (λ_{exc} = 488 nm, nominal power 50 mW) used for excitation. The white light probe passed through a first monochromator (Acton SpectraPro by Princeton Instruments) before being focused on the sample in a spot of 0.5 cm^2. The light transmitted through the sample was focused onto a second monochromator and detected by a silicon photodiode connected to a Femto DLPCA-200 current amplifier and lock-in amplifier (Stanford Research System model SR 830). An intensity of ~15 mW/cm^2 and a modulation frequency of 170 Hz were used for the excitation laser.

Photovoltage transients were taken using a pump-pulse generated by a InnoLas tunable laser at a rate of 1 Hz (OPO, 6 ns pulse fwhm). Excitation was provided at the absorption peak of each sample (i.e., 550 nm for G2-based solar cells). The pulse intensity was controlled to keep the variation of V_{oc} due to the pulse below 10 mV.

To simulate the 1.0 sun working condition, illumination was provided by nine white LEDs (Luxeon Star) with computer-controlled, tuned intensity. The cells were connected to a data acquisition (DAQ) card that allowed measurement of the steady state and of the transient voltage/current, as well as the selection of open- or short-circuit condition. Open circuit voltages and short circuit currents were measured over a GΩ and 2 Ω resistor, respectively.

RESULTS AND DISCUSSION

Photovoltaic Performances. The four sensitizers were employed in liquid electrolyte DSSC devices, and their performances were investigated both in terms of $J-V$ characteristics and of incident photon-to-current efficiency (IPCE). The main PV parameters reported in Table 1 and the

Table 1. Main PV Parameters of DSSC Devices Based on, G1, G2, DTB-B, and DTB-T Measured under 1.0 sun Illumination (AM 1.5, 100 mW cm^{-2})

dye	PCE (%)	V_{oc} (V)	J_{sc} (mA/cm^2)	FF
DTB-B	3.0	0.63	6.03	0.78
DTB-T	3.5	0.65	6.86	0.77
G1	6.0	0.69	12.2	0.71
G2	8.1	0.71	15.8	0.72

$I-V$ curves shown in Figure 2a have been obtained by dyeing the photoanodes in the presence of a 80 mM concentration of CDCA, which was found to be the optimal amount to maximize performances of G1 and G2.[16] The efficiencies obtained for DTB-T and DTB-B (3.0% and 3.5% respectively), albeit low, are remarkable considering that these are donor-free sensitizers with considerably low molar absorptivity. The lower photon-to-current efficiency of DTB-T and DTB-B can mainly be ascribed to the lower photocurrent, the fill-factors being very similar and the V_{oc} being only slightly lower with respect to G1 and G2; on the other hand, the efficiencies of the main sensitizer were 6.0% and 8.1%, respectively

The superior J_{sc} value for G1 and G2 also emerged from the IPCE spectra (Figure 3b), which showed good conversion efficiencies in the whole range comprised between 400 and 700 nm.

An insight into the PV behavior of the four sensitizer was performed by a complete set of spectroscopic measurements to monitor charge generation and recombination dynamics for the four sensitizers, embedded in simplified working devices (see the Experimental Section) and/or in model samples. The performances of the simplified working devices are reported in the Supporting Information (Table S1).

We studied charge generation and recombination with time-correlated single photon counting (TCSPC), continuum wavelength photoinduced absorption (cw-PIA), transient

DOI: 10.1021/jp5121004
J. Phys. Chem. C 2015, 119, 6956−6965

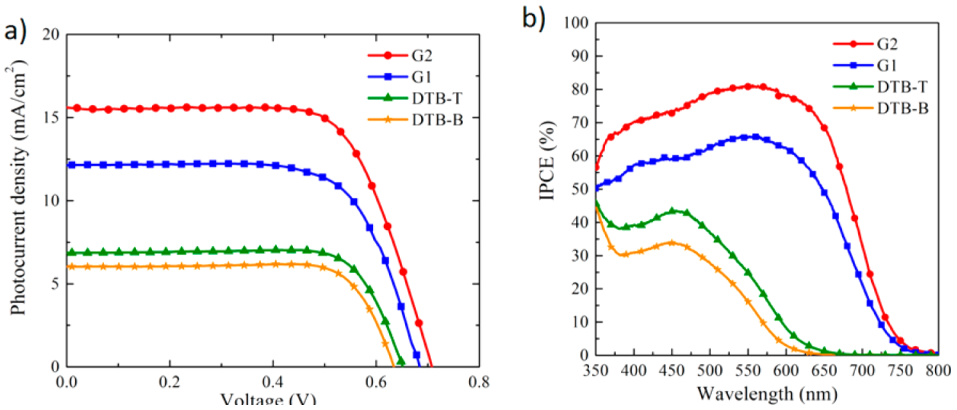

Figure 2. (a) $I-V$ curves of the devices summarized in Table 1 and (b) IPCE spectra.

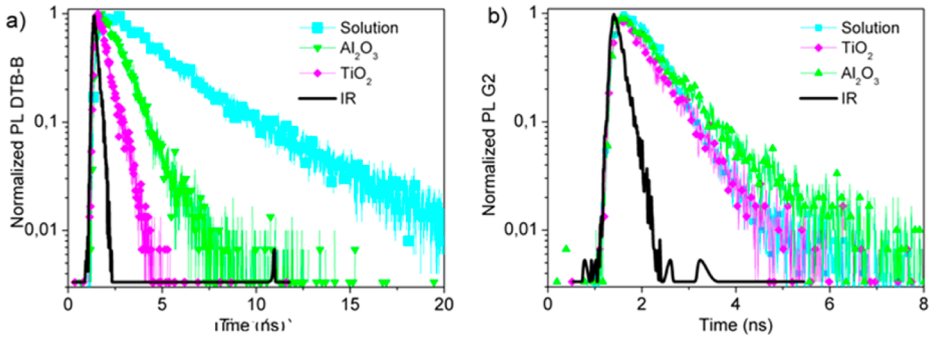

Figure 3. PL decay observed in diluted solution (0.01 mM), in electron-injecting (TiO_2-based) and noninjecting (Al_2O_3-based) devices observed for the two sensitizers. IR refers to the instrumental response to the laser input. (a) PL decay of DTB-B collected above 550 nm with high pass filter. (b) PL decay of G2 collected above 700 nm. The steady-state emission profiles for the four sensitizers are reported in Figure S1 of the Supporting Information.

absorption (TA), transient photovoltage–photocurrent analysis, and electrochemical impedance spectroscopy (EIS).

Charge Injection Analysis. Photoexcited electron injection in TiO_2 was investigated by monochromatic time-resolved photoluminescence using time-correlated single photon counting (TCSPC) equipment, a standard procedure for the determination of charge generation efficiency in both liquid electrolyte and solid-state dye-sensitized solar cells, as well as in nanocrystal-sensitized solar cells (see Supporting Information for further details).[18−20] For our purpose, apart from the photoanode, both cell have been assembled (see Experimental Section), reproducing a complete device, i.e., by using the same platinum counter electrode and the same electrolyte. Under these conditions, the injection mechanism can properly be isolated from other photophysical processes and the injection efficiency (η_{inj}) retrieved from time constant analysis by applying eqs 1 and 2,[21,22] in which $k_0 = 1/\tau_0$ is obtained from the PL decay of the dye in the noninjecting cell and $k_{obs} = 1/\tau_{obs}$ from the analogous data obtained from the electron-injecting cell.

$$\eta_{inj} = \frac{k_{inj}}{k_{inj} + k_0} \quad (1)$$

$$k_{inj} + k_0 = k_{obs} \quad (2)$$

The main complication arising in the TCSPC analysis of organic dyes is the PL self-quenching due to aggregation of dye molecules on the surface, which generates a further luminescence deactivation path that is not easily separable from the injection process.[20,22] Although cells for the measurements were assembled using a much more diluted dye solution (10 times more diluted than in a standard working cell) while the dye/CDCA ratio was kept constant, in some cases the effect of aggregation could not be avoided and contributed to PL quenching in such a way that injection efficiency was underestimated. In fact, in our experiment the aggregation effect is reasonably present both in the Al_2O_3 and in the TiO_2 samples, but it majorly affects the determination of dye lifetime on inert substrate. In fact, in the case of Al_2O_3 samples, the decay time is expected to be longer, falling well within our measurement window; meanwhile, the injecting substrate (TiO_2) is usually characterized, even for unaggregated dyes, by a very short radiative lifetime, lying below our instrumental resolution. The consequence of this technical limitation is the underestimate of the injection rate when eqs 1 and 2 are applied with the retrieved lifetimes. Here we report the results obtained for G2 and DTB-B dyes, employed to study the effect of the donor group on the better-performing dye G2. The PL decay constants of the dyes dissolved in THF (0.01 mM concentration, in the presence of 4.0 mM CDCA) and anchored to injecting (TiO_2-based) and noninjecting (Al_2O_3-based) devices have been obtained by fitting the experimental curves with stretched exponential functions. The results are summarized in Table 2, while the measured decays are reported in Figure 3, together with the relevant fitting curves.

Concerning the donor-free DTB-B sensitizer, the retrieved 88% and 96% injection efficiencies calculated by comparing Al_2O_3 vs TiO_2 or solution vs TiO_2 systems, respectively, are

DOI: 10.1021/jp5121004
J. Phys. Chem. C 2015, 119, 6956−6965

Table 2. Summary of Decay Constants for the Dyes G2 and DTB-B Obtained from Stretch Exponential Fitting

dye	solution (ns)	Al_2O_3 τ_0 (ns)	TiO_2 τ_{obs} (ns)	relative η_{inj}
DTB-B	3.546	1.271	0.157	TiO_2 vs Al_2O_3, 88% TiO_2 vs solution, 96%
G2	0.829	0.705	0.691	

very high and comparable to the results usually obtained for highly performing dyes.[21] It is important to remark again how residual dye aggregation effects might be responsible for an underestimation of electron-injecting efficiency. This problem has been already discussed for other high-performing dyes that showed very low (around 50%) injection efficiencies when investigated with PL quenching analysis.[20,22]

Conversely, in the case of G2, a fast PL decay is observed even in diluted (10^{-5} M) solution. Moreover, no appreciable difference appears in the PL decay of the dye in electron-injecting and noninjecting samples. In the case of G2, it seems then that this technique is not suited for the calculation of injection efficiency. Indeed, after excluding dye aggregation and dipole−dipole interaction due to the high dilution and the presence of coadsorbent, the same observed PL lifetime for the two solid substrates points out a complication in the measurement approach. In fact, in the TiO_2-based electron-injecting device, an efficient charge injection is expected and actually observed (vide infra), as well as, consequently, a stronger PL quenching. The same is observed for the analogous dye G1 (see Figure S2, Supporting Information). This observation might be justified by taking into account the stereoelectronic features of G2 and G1, in which the presence of a strongly electron donating group (the triarylamine, bearing two further 2-ethylhexyloxy electron-donating substituents) might alter the excited state distribution of the dye, interfering with its radiative deactivation.[23] For G1 and G2, however, the same or even a higher injection efficiency compared with that of DTB-B can safely be hypothesized. In fact, the driving force for electron injection in these systems, given the same electrolyte composition, mainly depends on the energy offset of the LUMO of the sensitizers with respect to the TiO_2 conduction band.[24] From the reported LUMO values obtained by cyclic voltammetry experiments,[16,17] it is evident that DTB-B and DTB-T possess a low-lying LUMO level (−3.4 eV) respect to G1 and G2 (−3.2 and −3.1 respectively). A ∼3 factor in injection driving force has been associated with a 100 meV higher sensitizer excited state, considering an exponentially increasing density of acceptor states;[21] thus, a similar or even more efficient electron transfer dynamics for G1 and G2 dyes compared to DTB-B can safely be expected. These considerations are supported by IPCE and *I*−*V* results reported above, in which the high photocurrent obtained for the devices embedding G1 and G2 is evident.

In summary, the charge injection analysis carried out by TCSPC points out that charge generation seems to be neither limiting nor discriminating in the series of investigated sensitizers, since a remarkable 88% injection yield could be evaluated for DTB-B, the dye with the lowest LUMO energy level, notwithstanding residual dye aggregation effects. As a consequence, it can be concluded that the presence of the triarylamine group seems to have a minor role in the electron injection mechanisms, as confirmed also by the moderate efficiency values obtained (vide supra) for the donor-free dyes DTB-T and DTB-B.

Photoinduced Absorption. To directly monitor charge dynamics in the investigated systems, we performed a continuous wavelength (cw) photoinduced absorption (PIA) investigation on suitably prepared devices (see the Experimental Section). The cw-PIA[25] is a widely used tool for the determination of charge generation efficiency in both liquid electrolyte and solid-state dye-sensitized solar cells (see the Supporting Information for further details).

In Figure 4 the modulus of the PIA signal (sum of in-phase and out-of-phase signals from coupled lock-in filter) is reported

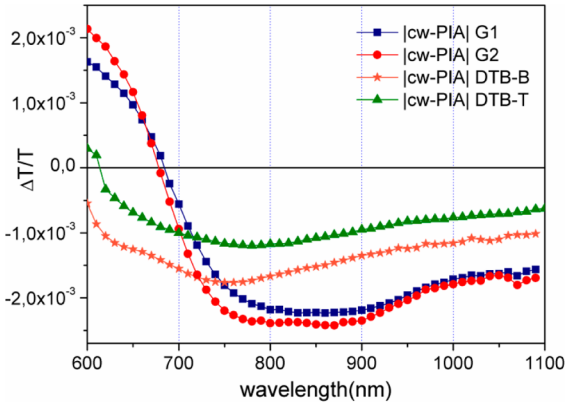

Figure 4. Modulus of photoinduced absorption spectra for G1, G2, DTB-T, and DTB-B in complete working devices. A 488 nm excitation laser was employed for all the samples, with 170 Hz chopper frequency.

for the all dyes in complete working DSSC devices. Samples for PIA measurements have a thinner working electrode (6 μm) due to the transmission nature of the analysis. Performances of such cells (see Table S1, Supporting Information) are, of course, lower than the optimized one reported in Table 1; however, they have the same efficiency trend, keeping the comparison meaningful. Excitation was provided at the same wavelength for all the dyes, and a 488 nm laser was chosen since dyes showed almost the same molar absorptivity at this wavelength (see the absorption spectra reported in Figure S3, Supporting Information). Spectra were collected in a transmission experiment configured in order to show negative signals corresponding to the absorption of photogenerated species and positive signals corresponding to the bleaching of ground-state absorptions. It is evident from the PIA spectra that the better-performing dyes (G1 and G2) present a stronger negative signal in the 700−1100 nm region compared to the worse-performing dyes (DTB-B and DTB-T). In this vis−NIR region, electrons injected in the TiO_2 matrix are absorbing with known cross-section.[26] This result can, in principle, indicate for the two standard D−A−π−A dyes both higher electron injection efficiency in TiO_2 and slower recombination rate for photogenerated charges, since, provided that the absorption cross section is the same for photoinduced species, the amplitude of each signal is a product of species recombination lifetime and the amount of absorbers. As previously discussed, injection efficiency cannot be considered a limiting or discriminating factor in the series of sensitizers; therefore, a major difference in the electron recombination dynamics is expected, highlighted by stronger photoinduced absorption for TiO_2 electrons for G1- and G2-based DSSC, which are

DOI: 10.1021/jp5121004
J. Phys. Chem. C 2015, 119, 6956−6965

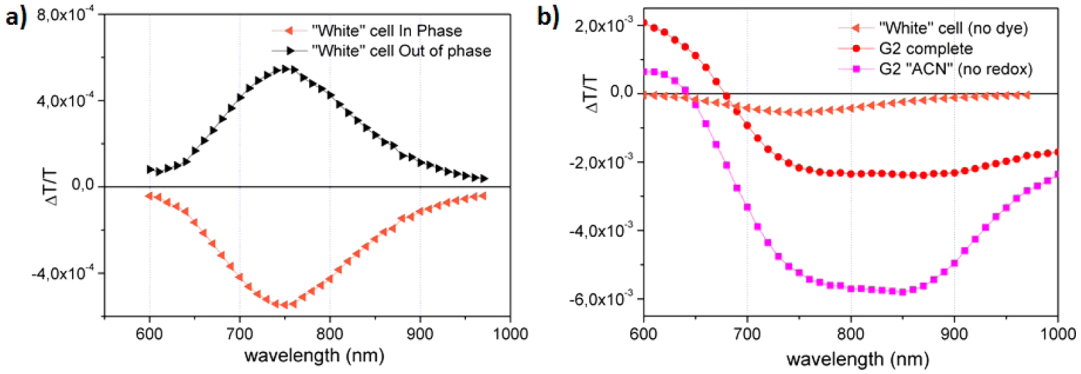

Figure 5. (a) In-phase (orange triangle) and out-of-phase (black triangle) photoinduced absorption spectra of a white cell (unsensitized TiO_2 substrate with electrolyte). (b) In-phase photoinduced absorption spectra of the building blocks of a working device employing G2 dye (i.e., ACN cell embedding the dye on the substrate and the solvent, acetonitrile, without the redox couple, pink squares), a white cell (i.e., no dye, orange triangles, same as Figure 5a), and a complete G2 cell (red dots), under the same experimental conditions as those reported in Figure 4.

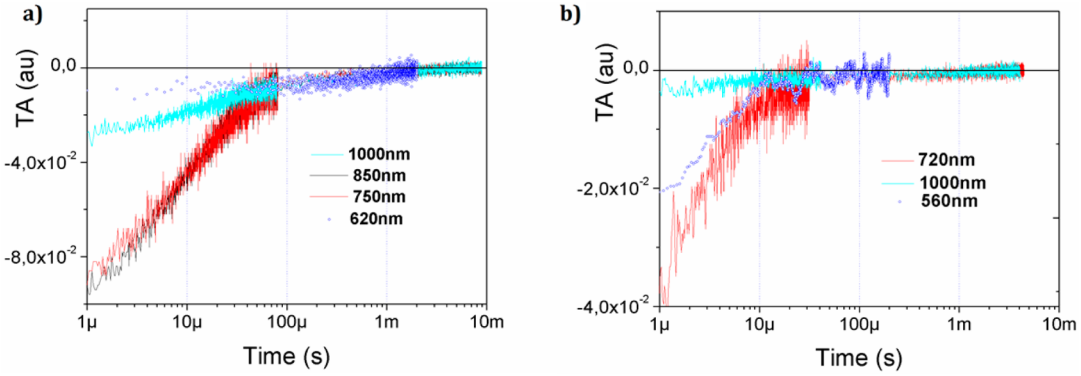

Figure 6. (a) Transient absorption of G2-based, simplified working devices. Signals are collected at selected wavelengths: 1000 nm (electrons in TiO_2), 850 nm (oxidized dye), 750 nm ($I_2^{-\bullet}$ species), and 620 nm (ground-state absorption of G2). (b) Transient absorption of DTB-B-based, simplified working devices under the same conditions. Signals are collected at selected wavelengths: 1000 nm (electrons in TiO_2), 720 nm ($I_2^{-\bullet}$ species), and 560 nm (ground state absorption of DTB-B). A 532 nm ns pulsed laser was employed for excitation of both samples.

expected to show a very long dynamics. Further evidence will be provided in the following to corroborate this hypothesis.

In order to properly assign the diverse features of cw-PIA to the absorption of the various photogenerated species, we carried out the investigation on suitable samples constituted by isolated cell components: (1) a complete working cell prepared as described in the Experimental Section, (2) a "white" cell constituted by a device embodying an unsensitized photoanode that was assembled to the counter electrode as described for the working device, and (3) a G2-sensitized "ACN" cell in which no redox couple in the liquid media was present. The results are reported in Figure 5. Figure 5a displays the results of the PIA measurement, under the same conditions as Figure 4, for the electrolyte filling a cell with nonsensitized substrate. The presence of the known redox precursor $I_2^{-\bullet}$ [27] is observed as an absorption feature, peaking at 750 nm, following electrolyte excitation, even in absence of the sensitizer. The amplitude of this signal is frequently monitored in photoinduced absorption analysis, being a fingerprint of dye regeneration efficiently taking place.[28]

Figure 5b reports the example of the G2 cell in its "building blocks", i.e., an ACN cell (only acetonitrile and no redox couple) and a white cell without dye (same as panel a), and the G2-sensitized complete cell. Comparing the three curves, negative features around 750 and 850 nm are attributed to the absorption of oxidized dye; in fact, in the complete device they disappear after regeneration, and only a small shoulder around 750 nm remains visible (where also the electrolyte transient species is absorbing, as already observed). In the complete device only this shoulder gives a negative contribution, together with the broad signal of electrons injected in TiO_2 (700−1000 nm). The positive signal at ca. 600 nm is assigned to the ground-state bleaching of the dye and it is still visible after dye regeneration because of the superposition of Stark features. These features are due to a local electric field generated by electrons injected in TiO_2 perturbing ground-state absorption of the dye.[29]

Charge Recombination Analysis. In order to provide more insight into the charge recombination processes occurring in the devices embodying our dyes, measurement of transient absorption (TA) was carried out. In TA measurements, the excitation is provided by a nanosecond pulsed laser, while a continuum beam from the monochromatic lamp probes selected spectral regions. With this technique, the exponential decay of photogenerated species can directly be observed, so their recombination in the microsecond to second time regime is accurately monitored.[30] The comparison of transient absorption signals collected for G2 and DTB-B at significant wavelengths is reported in parts a and b of Figure 6, respectively.

Figure 6a shows four TA decays for G2, corresponding to the absorption dynamics of electrolyte redox precursor $I_2^{-\bullet}$ (750

DOI: 10.1021/jp5121004
J. Phys. Chem. C 2015, 119, 6956−6965

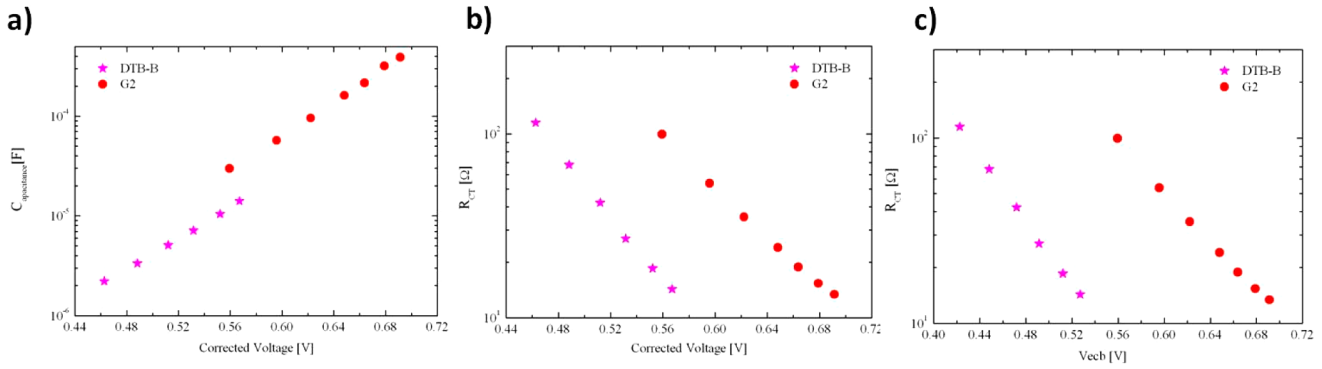

Figure 7. Impedance results of the DSSCs based on DTB-B and G2 dyes. (a) Measured capacitance vs corrected voltage. (b) Charge transfer resistance vs corrected voltage. (c) Charge transfer resistance represented at the equivalent CB position.

nm), oxidized dye (850 nm), dye absorption bleaching (620 nm), and TiO_2 electrons (1000 nm; see Figure 5a,b for comparison). The two dynamics at 750 and 850 nm are superimposed, because both signals monitor dye regeneration. The signal collected at 1000 nm shows the very long dynamics of electrons in the TiO_2 matrix, living up to 10 ms, as already hypothesized when reporting results for PIA measurements (Figure 4). The signal collected at 620 nm should follow the dynamics of ground-state bleaching, as should the signal of oxidized dye (850 nm), since regeneration should be as fast as ground-state-bleaching recovery. This signal, instead, appears as long as the signal from electrons in TiO_2 (1000 nm); this phenomena has already been observed and attributed to Stark effects superimposed on PIA signals, induced by electrons injected in the oxide matrix.[29,31]

Noticeably, a long (ms) transient component is present at every investigated wavelength, in both samples, since electrons in TiO_2 absorb in the whole investigated spectral range (600−1000 nm), and comparison between dynamics has been carried out by superimposing this long-living signal.

Panel b shows the dynamics for DTB-B; in this case, signals were collected at 720 nm (electrolyte redox precursor) and 1000 nm (electrons in TiO_2), and signals for dye absorption bleaching (560 nm) were notably positioned differently from that of the extended sensitizer (G2) due to the relative absorption shift (see Figure S3, Supporting Information). The decay at 720 nm was reported instead of the one at 750 nm, because the latter, despite being similar in terms of profile, was affected by strong electrical noise; the comparison remains meaningful as the monitored species shows a wide absorption band (Figure 5a). In addition, for this dye it was not possible to evidence the absorption of the oxidized species. The comparison shows that both the dynamics attributed to the dye regeneration (720 nm) and that attributed to electrons recombination (1000 nm) are faster in the case of this dye compared to G2. Absorption of $I_2^{-\bullet}$ shows a dynamics of about 100 μs for G2 and 10 μs for DTB-B, while TiO_2 electrons present a lifetime as long as 10 ms in G2-sensitized devices and less than 1 ms for DTB-B-sensitized ones. In other words, regeneration seems to be favorable for DTB-B because it is completed in shorter time, but at the same time, recombination of TiO_2 electrons is faster, providing shorter carrier lifetime. The signal associated with ground-state bleaching follows in this case the dynamics of the oxidized dye, indicating that in this case the Stark effect could be less intense. The reason for this observation might reside in the higher permanent dipole due to the presence of the donor moiety, so the perturbation of the local electric field is more evident.

Electrons injected in TiO_2 can recombine with oxidized dye or with the oxidized species of the electrolyte redox couple, and in the case under exam, cannot quantitatively distinguish between these two phenomena. Nevertheless it can be hypothesized that the triarylamine electron-donating group is acting as a "barrier", interfering with both dye regeneration and electrons/electrolyte recombination processes because of its steric hindrance. The overall performances of the cell are majorly affected by the detrimental recombination increase rather than the beneficial dye regeneration improvement; thus, the PV performances of dyes G1 and G2 are almost double compared to their donor free counterparts (DTB-T and DTB-B, respectively).

For a better understanding of the origin of the analyzed behavior, we examined the electron recombination processes within the PV cell by means of electrochemical impedance spectroscopy (EIS), carried out at different voltage biases under 1.0 sun illumination (see the Supporting Information for further details).[32,33]

Figure 7a,b show the capacitance and recombination resistance as a function of potential drop at the sensitized electrode. V_{corr} is obtained by correcting the applied potential (V_{app}) with the drop of total series resistance V_{series} (contacts, counter electrode, electrolyte diffusion) collected from impedance spectroscopy data by $V_{corr} = V_{app} - V_{series}$.[33] The chemical capacitance, C_μ, represented in Figure 7a, provides quantitative information on the position of the conduction band as[34]

$$C_\mu = \frac{e^2}{k_B T} \exp\left[\frac{\alpha}{k_B T}(E_{F_n} - E_{CB})\right] \quad (3)$$

where e is the electron charge, k_B is the Boltzmann constant, T is the absolute temperature, E_{F_n} is the position of the Fermi level of electrons, E_{CB} is the energy of the conduction band, and α is a constant related to the distribution of electronic states below the conduction band. Figure 7a shows that chemical capacitance values are clearly shifted toward lower potentials for G2 dye. Assuming that neither the distribution nor the total amount of trap states changed the dye, we may attribute the shift observed in C_μ to a displacement in the energy of the conduction band (CB).[33] The downward shift of the TiO_2 CB influences the PV performance of the solar cell by increasing J_{sc} values due to the higher electron-injection driving force and, on the other hand, by decreasing V_{oc} due to a reduction of the

DOI: 10.1021/jp5121004
J. Phys. Chem. C 2015, 119, 6956−6965

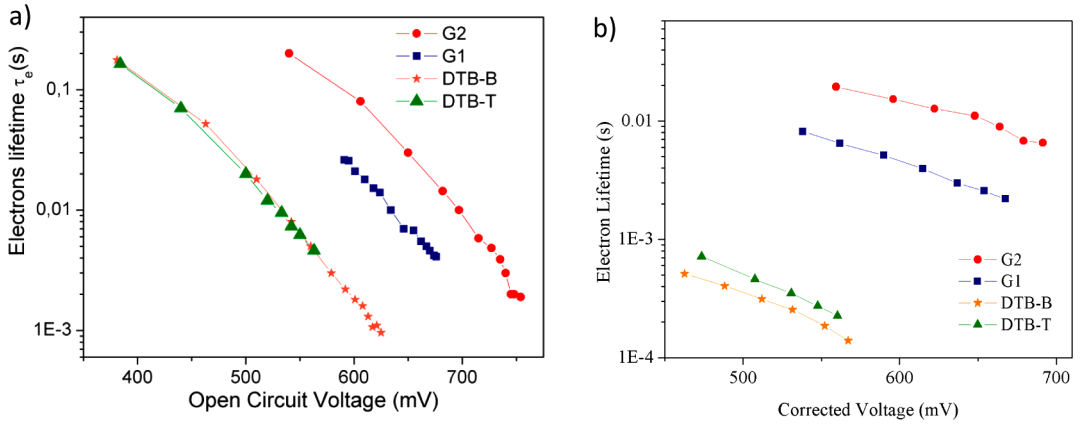

Figure 8. Electron lifetime (a) as a function of open circuit voltage, derived from exponential fitting of transient photovoltage decays at modulated light intensity, and (b) derived from impedance spectroscopy for G1, G2, DTB-T, and DTB-B.

difference between the TiO_2 Fermi level and redox potential. However, inspection of Table 1 reveals that both V_{oc} and J_{sc} of the G2-based cell are higher than those of the DTB-B-based cell. These parameters should be controlled by the inhibited recombination and thus improved J_{sc}, which will be analyzed in detail below.

Figure 7b shows the recombination resistance plotted versus potential drop at the sensitized electrode. According to the Marcus theory,[35] electron transfer between TiO_2 and the redox acceptor (i.e., recombination current) can occur only between levels at the same energy. Taking this into account, it is reasonable to expect that the higher the conduction band, the lower the recombination current (J_{rec}) and, therefore, the higher the recombination resistance (R_{ct}) (eq 4) due to the lower amount of electrons available to recombine.

$$R_{ct} = \left(\frac{\partial J_{rec}}{\partial V}\right)^{-1} \tag{4}$$

However, as shown in Figure 7b, the DTB-B-based cell shows lower charge transfer resistance than the G2-based cell, even if the latter shows a downward shift of the conduction band. The suppression of recombination in the G2-based devices with respect to the DTB-B-based ones might be attributed to the presence of a bulky triarylamine group, which contributes to the formation of a more robust organic layer uniformly covering the TiO_2 surface in the former. The difference in charge transfer resistance becomes more marked if the R_{ct} of the two devices is plotted against the voltage drop in a common equivalent conduction band (V_{ecb}).[36] In this plot (Figure 7c) the effect of different TiO_2 CB between samples is removed. This allows an analysis of the recombination resistance on the basis of an equal density of electrons n (i.e., the same distance between the electron Fermi level and the TiO_2 CB).

In order to further rationalize recombination mechanisms in the model DSSC devices based on G1, G2, DTB-T, and DTB-B, we performed transient photovoltage (TPV) measurements. This technique is employed for the determination of electron lifetimes (τ_e) in DSSCs. For a cell held at open circuit (V_{oc}), the concentration of carriers in the charge-transporting matrix is varied by applying a tunable bias light, while a short, weak laser pulse determines an additional amount of generated charge. The transient photovoltage associated with this population perturbation is related to electron recombination processes.[37,38]

The electron recombination lifetime is calculated by fitting the transient photovoltage decay with single-exponential functions. The extracted τ_e is shown in Figure 8, as a function of the open-circuit voltage on complete working devices.

Comparison of charge recombination rate is performed at the same V_{oc} (Figure 8). A clear trend is evidenced by the measurement, with G2 showing longer electron recombination lifetime, followed by G1 and with the two donor-free dyes showing the same faster dynamics. This result corroborates the observation of shorter carriers lifetime in the DTB-T- and DTB-B-based, worse-performing devices, demonstrated by cw-PIA experiments.

Figure 8 shows the electron lifetime curves obtained from the exponential fitting of transient photovoltage decays (Figure 8a) and from EIS measurements (Figure 8a). The electron lifetime (τ), obtained from EIS measurement, is usually calculated from R_{ct} and C_μ by using the equation

$$\tau = R_{ct}C_\mu \tag{5}$$

Noticeably, the electron lifetimes follow the same trend, and the difference in the absolute values is due to the experimental conditions differing in the two cases. Transient photovoltage decays were obtained at open circuit potential via modulating the light intensity, whereas impedance spectroscopy was performed at 1.0 sun and the modulation was on the applied potential. Compared to the other devices, the G2-based one showed the most prolonged electron lifetime at any bias, substantiating its better PV performances.

The sum of these results confirms that the different PV performances observed for G1, G2, DTB-T, and DTB-B could be rationalized in term of different electron recombination dynamics. The bulky donor moiety is preventing massive charge recombination for G1- and G2-based devices by protecting the TiO_2 interface from electrolyte contact, as showed in PIA, TA, TPV, and EIS analyses. The same measurements show how the presence of a phenyl ring replacing the thiophene group in the π-extension region of the dye implies better PV performances for G2-based devices in comparison with G1-based ones. We hypothesize that the presence in the latter of a thiophene sulfur atom close to the TiO_2 surface, by favoring interactions with the triiodide in the electrolyte, triggers detrimental recombination pathways.[39,40]

DOI: 10.1021/jp5121004
J. Phys. Chem. C 2015, 119, 6956−6965

CONCLUSIONS

Two D−A−π−A organic dyes, G1 and G2, are spectroscopically investigated and compared with their donor-free congeners, DTB-T and DTB-B. Charge generation is proved not to be a limitation nor a discriminating factor among the series, as we observed remarkable electron injection yields for all dyes. Dye regeneration and electron recombination, instead, are found to vary significantly, and this evidence is justified by the presence of triarylamine electron-donating group acting as a "barrier", interfering with both processes due to its steric hindrance. The overall performances of the DSSC are majorly affected by the detrimental increase in recombination rather than the beneficial improvement in dye regeneration; thus, the PV performances of dyes G1 and G2 are almost doubled with respect to that of their donor-free congeners (DTB-T and DTB-B, respectively). Both TPV and EIS results confirm longer electron lifetimes for G2 with respect to G1. The different performances recorded between the two D−A−π−A dyes G1 and G2 have therefore to be related to their different recombination in devices. The two dyes differ from the presence of a thiophene instead of a benzene moiety, and the presence of a sulfur atom is most probably the detrimental element justifying the worse performances of G1. The collection of our results relating the sensitizer structure with the PV performance of dye-including devices is very useful for the future rational design of novel D−A−π−A sensitizers.

ASSOCIATED CONTENT

Supporting Information

Further details on spectroscopic and electrochemical characterizations. This material is available free of charge via the Internet at http://pubs.acs.org/.

AUTHOR INFORMATION

Corresponding Author

*E-mail: andrea.listorti@iit.it. Tel: +3908321816241.

Notes

The authors declare no competing financial interest.

ACKNOWLEDGMENTS

This work was supported by EFOR (Iniziativa CNR per il Mezzogiorno L. 191/2009 art. 2 comma 44), by PON-MAAT (Project Number: PON02_00563_3316357-CUP B31C12001230005), by PONFORM@BEYOND-NANO, and by Regione PUGLIA (APQ Reti di Laboratorio, project "PHOEBUS" cod. 31).

REFERENCES

(1) IEA. *World Energy Outlook 2013*; OECD/IEA: Paris, 2013.
(2) O'Regan, B.; Grätzel, M. A Low-Cost, High-Efficiency Solar Cell Based on Dye-Sensitized Colloidal TiO_2 Films. *Nature* **1991**, *353*, 737−739.
(3) Hagfeldt, A.; Boschloo, G.; Sun, L.; Kloo, L.; Pettersson, H. Dye-Sensitized Solar Cells. *Chem. Rev.* **2010**, *110*, 6595−6663.
(4) Jung, H. S.; Lee, J.-K. Dye Sensitized Solar Cells for Economically Viable Photovoltaic Systems. *J. Phys. Chem. Lett.* **2013**, *4*, 1682−1693.
(5) O'Regan, B. C.; Durrant, J. R. Kinetic and Energetic Paradigms for Dye-Sensitized Solar Cells: Moving from the Ideal to the Real. *Acc. Chem. Res.* **2009**, *42*, 1799−1808.
(6) Gao, F.; Wang, Y.; Shi, D.; Zhang, J.; Wang, M.; Jing, X.; Humphry-Baker, R.; Wang, P.; Zakeeruddin, S. M.; Grätzel, M. Enhance the Optical Absorptivity of Nanocrystalline TiO_2 Film with High Molar Extinction Coefficient Ruthenium Sensitizers for High Performance Dye-Sensitized Solar Cells. *J. Am. Chem. Soc.* **2008**, *130*, 10720−10728.
(7) Snaith, H. J.; Humphry-Baker, R.; Chen, P.; Cesar, I.; Zakeeruddin, S. M.; Grätzel, M. Charge Collection and Pore Filling in Solid-State Dye-Sensitized Solar Cells. *Nanotechnology* **2008**, *19*, 424003.
(8) Bai, Y.; Cao, Y.; Zhang, J.; Wang, M.; Li, R.; Wang, P.; Zakeeruddin, S. M.; Grätzel, M. High-Performance Dye-Sensitized Solar Cells Based on Solvent-Free Electrolytes Produced from Eutectic Melts. *Nat. Mater.* **2008**, *7*, 626−630.
(9) Mishra, A.; Fischer, M. K. R.; Bäuerle, P. Metal-Free Organic Dyes for Dye-Sensitized Solar Cells: From Structure: Property Relationships to Design Rules. *Angew. Chem., Int. Ed.* **2009**, *48*, 2474−2499.
(10) Ahmad, S.; Guillén, E.; Kavan, L.; Grätzel, M.; Nazeeruddin, M. K. Metal Free Sensitizer and Catalyst for Dye Sensitized Solar Cells. *Energy Environ. Sci.* **2013**, *6*, 3439.
(11) Joly, D.; Pellejà, L.; Narbey, S.; Oswald, F.; Chiron, J.; Clifford, J. N.; Palomares, E.; Demadrille, R. A Robust Organic Dye for Dye Sensitized Solar Cells Based on Iodine/Iodide Electrolytes Combining High Efficiency and Outstanding Stability. *Sci. Rep.* **2014**, *4*, 4033.
(12) Wu, Y.; Zhu, W. Organic Sensitizers from D−π−A to D−A−π−A: Effect of the Internal Electron-Withdrawing Units on Molecular Absorption, Energy Levels and Photovoltaic Performances. *Chem. Soc. Rev.* **2013**, *42*, 2039−2058.
(13) Wu, Y.; Marszalek, M.; Zakeeruddin, S. M.; Zhang, Q.; Tian, H.; Grätzel, M.; Zhu, W. High-Conversion-Efficiency Organic Dye-Sensitized Solar Cells: Molecular Engineering on D−A−π−A Featured Organic Indoline Dyes. *Energy Environ. Sci.* **2012**, *5*, 8261.
(14) Haid, S.; Marszalek, M.; Mishra, A.; Wielopolski, M.; Teuscher, J.; Moser, J.-E.; Humphry-Baker, R.; Zakeeruddin, S. M.; Grätzel, M.; Bäuerle, P. Significant Improvement of Dye-Sensitized Solar Cell Performance by Small Structural Modification in π-Conjugated Donor−Acceptor Dyes. *Adv. Funct. Mater.* **2012**, *22*, 1291−1302.
(15) Lee, D. H.; Lee, M. J.; Song, H. M.; Song, B. J.; Seo, K. D.; Pastore, M.; Anselmi, C.; Fantacci, S.; De Angelis, F.; Nazeeruddin, M. K.; et al. Organic Dyes Incorporating Low-Band-Gap Chromophores Based on π-Extended Benzothiadiazole for Dye-Sensitized Solar Cells. *Dyes Pigm.* **2011**, *91*, 192−198.
(16) Grisorio, R.; De Marco, L.; Agosta, R.; Iacobellis, R.; Giannuzzi, R.; Manca, M.; Mastrorilli, P.; Gigli, G.; Suranna, G. P. Enhancing Dye-Sensitized Solar Cell Performances by Molecular Engineering: Highly Efficient π-Extended Organic Sensitizers. *ChemSusChem* **2014**, 1−12.
(17) Agosta, R.; Grisorio, R.; De Marco, L.; Romanazzi, G.; Suranna, G. P.; Gigli, G.; Manca, M. An Engineered Co-Sensitization System for Highly Efficient Dye Solar Cells. *Chem. Commun.* **2014**, *50*, 9451−9453.
(18) Listorti, A.; O'Regan, B.; Durrant, J. R. Electron Transfer Dynamics in Dye-Sensitized Solar Cells. *Chem. Mater.* **2011**, *23*, 3381−3399.
(19) Bang, J. H.; Kamat, P. V. Quantum Dot Sensitized Solar Cells. A Tale of Two Semiconductor. *ACS Nano* **2009**, *3*, 1467−1476.
(20) Snaith, H. J.; Petrozza, A.; Ito, S.; Miura, H.; Grätzel, M. Charge Generation and Photovoltaic Operation of Solid-State Dye-Sensitized Solar Cells Incorporating a High Extinction Coefficient Indolene-Based Sensitizer. *Adv. Funct. Mater.* **2009**, *19*, 1810−1818.
(21) Koops, S. E.; O'Regan, B. C.; Barnes, P. R. F.; Durrant, J. R. Parameters Influencing the Efficiency of Electron Injection in Dye-Sensitized Solar Cells. *J. Am. Chem. Soc.* **2009**, *131*, 4808−4818.
(22) Listorti, A.; López-Duarte, I.; Martínez-Díaz, M. V.; Torres, T.; DosSantos, T.; Barnes, P. R. F.; Durrant, J. R. Zn(II) versus Ru(II) Phthalocyanine-Sensitised Solar Cells. A Comparison between Singlet and Triplet Electron Injectors. *Energy Environ. Sci.* **2010**, *3*, 1573.
(23) Katono, M.; Wielopolski, M.; Marszalek, M.; Bessho, T.; Moser, J.; Humphry-baker, R.; Zakeeruddin, S. M.; Gra, M. Effect of Extended π- Conjugation of the Donor Structure of Organic D−A−π−A Dyes on the Photovoltaic Performance of Dye-Sensitized Solar Cells. *J. Phys. Chem. C* **2014**, *118*, 16486−16493.

DOI: 10.1021/jp5121004
J. Phys. Chem. C 2015, 119, 6956−6965

(24) Hara, K.; Sato, T.; Katoh, R.; Furube, A.; Ohga, Y.; Shinpo, A.; Suga, S.; Sayama, K.; Sugihara, H.; Arakawa, H. Molecular Design of Coumarin Dyes for Efficient Dye-Sensitized Solar Cells. *J. Phys. Chem. B* **2003**, *107*, 597−606.
(25) Boschloo, G.; Hagfeldt, A. Photoinduced Absorption Spectroscopy of Dye-Sensitized Nanostructured TiO_2. *Chem. Phys. Lett.* **2003**, *370*, 381−386.
(26) Tachibana, Y.; Moser, J. E.; Gra, M.; Klug, D. R.; Durrant, J. R.; Fe, Ä. P. Subpicosecond Interfacial Charge Separation in Dye-Sensitized Nanocrystalline Titanium Dioxide Films. *J. Phys. Chem.* **1996**, *3654*, 20056−20062.
(27) Zhu, H.; Hagfeldt, A.; Boschloo, G. Photoelectrochemistry of Mesoporous NiO Electrodes in Iodide/Triiodide Electrolytes. *J. Phys. Chem. C* **2007**, *111*, 17455−17458.
(28) Abate, A.; Petrozza, A.; Roiati, V.; Guarnera, S.; Snaith, H.; Matteucci, F.; Lanzani, G.; Metrangolo, P.; Resnati, G. A Polyfluoroalkyl Imidazolium Ionic Liquid as Iodide Ion Source in Dye Sensitized Solar Cells. *Org. Electron.* **2012**, *13*, 2474−2478.
(29) Cappel, U. B.; Feldt, S. M.; Schöneboom, J.; Hagfeldt, A.; Boschloo, G. The Influence of Local Electric Fields on Photoinduced Absorption in Dye-Sensitized Solar Cells. *J. Am. Chem. Soc.* **2010**, *132*, 9096−9101.
(30) Anderson, A. Y.; Barnes, P. R. F.; Durrant, J. R.; Regan, B. C. O. Quantifying Regeneration in Dye-Sensitized Solar Cells. *J. Phys. Chem. C* **2010**, *115*, 2439.
(31) Ardo, S.; Sun, Y.; Staniszewski, A.; Castellano, F. N.; Meyer, G. J. Stark Effects after Excited-State Interfacial Electron Transfer at Sensitized TiO_2 Nanocrystallites. *J. Am. Chem. Soc.* **2010**, *132*, 6696−6709.
(32) Bisquert, J. Theory of the Impedance of Electron Diffusion and Recombination in a Thin Layer. *J. Phys. Chem. B* **2002**, *106*, 325−333.
(33) Mora-Seró, I.; Bisquert, J. Breakthroughs in the Development of Semiconductor-Sensitized Solar Cells. *J. Phys. Chem. Lett.* **2010**, *1*, 3046−3052.
(34) Bisquert, J. Chemical Capacitance of Nanostructured Semiconductors: Its Origin and Significance for Nanocomposite Solar Cells. *Phys. Chem. Chem. Phys.* **2003**, *5*, 5360.
(35) Bisquert, J.; Marcus, R. A. Device Modeling of Dye-Sensitized Solar Cells. *Top. Curr. Chem.* **2014**, *352*, 325−395.
(36) Barea, E. M.; Zafer, C.; Gultekin, B.; Aydin, B.; Koyuncu, S.; Icli, S.; Santiago, F. F.; Bisquert, J.; Uni, M. Quantification of the Effects of Recombination and Injection in the Performance of Dye-Sensitized Solar Cells Based on N-Substituted Carbazole Dyes. *J. Phys. Chem. C* **2010**, *114*, 19840−19848.
(37) O'Regan, B. C. O.; Lenzmann, F.; Cuscn, D.; Cells, P.; Regan, B. C. O. Charge Transport and Recombination in a Nanoscale Interpenetrating Network of n-Type and p-Type Semiconductors: Transient Photocurrent and Photovoltage Studies of TiO_2. *J. Phys. Chem. B* **2004**, *108*, 4342−4350.
(38) Barnes, P. R. F.; Miettunen, K.; Li, X.; Anderson, A. Y.; Bessho, T.; Gratzel, M.; O'Regan, B. C. Interpretation of Optoelectronic Transient and Charge Extraction Measurements in Dye-Sensitized Solar Cells. *Adv. Mater.* **2013**, *25*, 1881−1922.
(39) Li, X.; Reynal, A.; Barnes, P.; Humphry-Baker, R.; Zakeeruddin, S. M.; De Angelis, F.; O'Regan, B. C. Measured Binding Coefficients for Iodine and Ruthenium Dyes; Implications for Recombination in Dye Sensitised Solar Cells. *Phys. Chem. Chem. Phys.* **2012**, *14*, 15421−15428.
(40) Planells, M.; Pellejà, L.; Clifford, J. N.; Pastore, M.; De Angelis, F.; López, N.; Marderc, S. R.; Palomares, E. Energy Levels, Charge Injection, Charge Recombination and Dye Regeneration Dynamics for Donor−Acceptor π-Conjugated Organic Dyes in Mesoscopic TiO_2 Sensitized Solar Cells. *Energy Environ. Sci.* **2011**, *4*, 1820−1829.

DOI: 10.1021/jp5121004
J. Phys. Chem. C 2015, 119, 6956−6965